EXTENSIONS OF THE CONCEPT OF SUCTION ANALOGY TO PREDICTION OF VORTEX LIFT EFFECT*

C. Edward Lan
Department of Aerospace Engineering
University of Kansas
Lawrence, Kansas

SUMMARY

Flow field data for a double delta wing at low speed were used to determine the location of a vortex action point. The result was found to be consistent with what was determined for a delta wing. In supersonic flow, the action point location was determined empirically. For a wing with rounded leading edges, an assumption for initial vortex separation was shown to be equivalent to initial leading-edge bubble separation for airfoils. A theoretical formulation by the section analogy to determine the delayed vortex separation on a cambered wing with rounded leading edges was presented. The method of suction analogy was further shown to be applicable to predicting the body vortex lift.

INTRODUCTION

Since Polhamus introduced the method of suction analogy for plane delta wings with sharp edges in subsonic and supersonic flows (refs. 1 and 2), various extensions of the method have been proposed and used successfully. For wings with nonzero tip chord, Lamar introduced the effect of side-edge vortex lift (ref. 3). When a vortex generated at the leading edge passes over some downstream planform area, additional lift is induced because of the vortex suction effect. This additional lift was incorporated into the method of suction analogy by Lamar as the augmented vortex lift (ref. 4). The latter may be positive as is the case for a cropped delta wing and a strake-wing configuration. Augmented vortex lift is negative for an arrow wing because of the lack of downstream area to receive the vortex action or to allow the reattachment of the vortex flow. For a noncambered wing, the vortex force was assumed to be acting at the leading edge and normal to the planform. However, for a positive-cambered wing, this assumption would produce too much thrust as compared with data. To allow for the determination of where the vortex force is acting, the concept of vortex action point was introduced (ref. 5). If the leading edge is rounded, the generation of vortex lift will be delayed. Kulfan presented a method to account for this effect for plane wings (refs. 6 and 7). Another method for the effect of rounded leading edges was developed by Carlson by using available experimental data (ref. 8).

The method of suction analogy has also been employed to calculate the roll damping of slender wings (ref. 9). The extension of it to calculating all lateral-directional characteristics of slender wings was made in reference 10. In reference 10, the effect of vortex breakdown was also incorporated by using a

---

*This work was supported by NASA Grant NSG 1629.

numerical scheme to extend the available data for delta wings. Finally, an unsteady lifting-surface theory was used in developing the method of unsteady suction analogy (ref. 11). The latter can be used for predicting dynamic stability derivatives of slender wings.

In this paper, the concept of vortex action point is reconsidered for subsonic and supersonic flows. In addition, Kulfan's concept for plane wings with rounded leading edges is correlated with viscous flow calculations for airfoils. The extension of the method for cambered wings is described next. Finally, it is shown that the method of suction analogy can be applied to predict the vortex lift of slender bodies.

SYMBOLS

c	local chord
C	sectional leading-edge singularity parameter $= \lim_{x \to x_{le}} \gamma(x)(x - x_{le})^{1/2}$
C_D	drag coefficient
c_{d_w}	sectional wave drag coefficient
c_ℓ	sectional lift coefficient
C_L	lift coefficient
C_m	pitching moment coefficient
C_N	body normal force coefficient based on maximum cross-sectional area
$c_{n,v}$	sectional normal force coefficient due to body vortex lift
$C_{N,vA}$	total augmented vortex normal force coefficient on a body
C_p	pressure coefficient
c_s	sectional leading-edge suction coefficient
c_{sf}	sectional side-force coefficient of a body
$C_{sf,N}$	total suction force coefficient produced by a body nose section
c_t	sectional leading-edge thrust coefficient
f	ratio of vortex-induced vertical velocity to the free stream (eq. (2))
h	vortex action point location on a body defined in eqs. (15) and (16)
ℓ_N	body nose length
M	Mach number

r vortex action point location measured from the leading edge (eq. (4)), or body radius

r_o leading-edge radius

V velocity

x_s body axial station at which the vortex separation starts

α angle of attack

α_1 sectional angle of zero lift

α_s angle of attack of initial vortex separation

β sideslip angle or wave angle

β_s oblique shock angle

γ ratio of specific heats or bounded vortex density

Λ sweep angle

ρ density

θ angular coordinate of a body (fig. 8)

θ_A angular location of the augmented vortex action point on a body (eq. 21)

θ_c angular location of the body vortex action point (eq. (15) and fig. 10)

Subscripts:

ℓ lower surface

ℓ_e leading edge

u upper surface

∞ free stream

CONCEPT OF VORTEX ACTION POINT

In developing the concept of vortex action point, flow field data in cross-flow planes are needed, see figure 1(a). It is assumed that the velocity distribution around the vortex in the longitudinal plane parallel to the free stream is the same as that in the cross-flow plane (fig. 1(b)). If a control surface (σ) is taken through the vortex center as shown in figure 1(c), the vortex force should be equal to the vertical component of the force due to the momentum transfer through the control surface σ. Since the vortex force acting on the wing is equal to $c_s q_\infty c$ by the suction analogy, it follows that the force acting on the

control volume is

$$-c_s c \frac{1}{2} \rho V_\infty^2 = \int_\sigma \rho V_z (\vec{V} \cdot d\vec{\tau})$$

$$= \int (\rho V_{z_{in}} - \rho V_{z_{out}}) \vec{V} \cdot d\vec{t} \qquad (1)$$

To find an average $\vec{V}$, let

$$|\vec{V}| = V_z = fV_\infty \qquad (2)$$

where f is a constant. It follows that for a unit span,

$$\int (\rho V_{z_{in}} - \rho V_{z_{out}}) \vec{V} \cdot d\vec{t} = -fV_\infty [\int \rho V_{z_{in}} dr + \int \rho V_{z_{out}} dr]$$

$$= -fV_\infty 2\rho (fV_\infty) r \qquad (3)$$

where the integrals have been replaced with the average values. From equations (1) and (3), it is found that

$$r = \frac{1}{4f^2} c_s c \qquad (4)$$

In reference 5, f was taken to be 0.5 so that $r = c_s c$. To show that this choice of f is reasonable in subsonic flow, the flow field data in reference 12 for a double delta wing at station (1) are rearranged in figure 2. By numerically integrating the velocity distribution to evaluate the integrals in equation (3), an average velocity with f = 0.53 can be found. At station (2), the two leading-edge vortices have started to merge, so that the flow field data are not appropriate for the present purpose.

In supersonic flow, Squire et al. demonstrated by a vapor screen method that the vortex region became much flatter than that in subsonic flow (ref. 13), as shown in figure 3. Unfortunately, flow field velocity data are not available in reference 13 and, in fact, have not been found so far for other wing planforms. Therefore, an empirical method to determine an appropriate f value was used. By assuming different values for $1/4f^2$ and comparing the calculated C_L and C_D values with data for different planforms with leading-dege flaps, it was found that a value of 8.0 for $1/4f^2$ produced the best results. In other words, $f = 1/4\sqrt{2}$. Therefore, unless additional data prove otherwise, the following relation for the vortex action point will be used in supersonic flow:

$$r = 8(c_s c) \qquad (5)$$

Some calculated results are compared with data in figures 4 and 5 (refs. 14 and 15). It is seen that the theory predicts the results quite well. Note that the effect of rounded leading edges accounted for in figures 4 and 5 will be discussed in the next section. The wave drag correction in figures 4 and 5 is to add the nonlinear effect to the predicted linear values based on the predicted sectional lift coefficients and the exact two-dimensional theory for a flat plate in supersonic flow. The wave drag correction is described in the Appendix.

VORTEX LIFT ON CAMBERED WINGS WITH ROUNDED LEADING EDGES

Kulfan assumes that on a slender wing the leading-edge vortex separation starts at an angle of attack at which the leading-edge drag equals the leading-edge thrust (refs. 6 and 7). To examine this assumption, experimental pressure data (ref. 16) and theoretical results from the Lockheed-Georgia airfoil code (ref. 17) were used. The airfoil negative pressure coefficient is integrated to give the leading-edge suction ($c_{s_{\ell e}}$), and the positive pressure coefficient is integrated to produce the leading-edge drag ($c_{d_{\ell e}}$). The integration is over the forward portion of the airfoil from the maximum thickness location if no separation bubble occurs. Otherwise, the integration is performed only over the region forward of the separation bubble. The results indicate that at the angle of attack (α_s) at which the separation bubble first occurs, the leading-edge thrust is about equal to the leading-edge drag (ref. 18). For symmetrical airfoils, this is illustrated in figure 6. For cambered airfoils, some calculated results are presented in figure 7. As shown, the leading-edge suction at α_s tends to be greater than the leading-edge drag. This is due to the pressure thrust generated on the forward camber. To remove this camber thrust in performing the pressure integration, the slope of the upper airfoil surface is reduced by the local camber slope and that of the lower surface is increased by it. The results indicated in figure 7 by rectangular symbols (▯) show that Kulfan's concept is still applicable for cambered airfoils if the camber thrust is removed from the calculated suction. In the thin airfoil or wing theory, this is always true because the calculated leading-edge thrust is concentrated at the leading edge and does not contain the camber thrust.

Having established that Kulfan's concept on the starting of a leading-edge vortex separation is related to the occurrence of leading-edge laminar separation, the next question is how this concept can be used in calculating the vortex lift on a cambered wing with rounded leading edges. The first task is to determine α_s. For a cambered wing, the sectional leading-edge suction coefficient can be written as

$$c_s = K(\sin\alpha + \alpha_1)^2 \tag{6}$$

where K is a function of geometry and Mach number, and α_1 is the sectional angle of zero lift. In practice, α_1 can be found as follows. Let c_s' be the sectional leading-edge suction coefficient for the same wing without camber. Then

$$c_s' = K \sin^2\alpha \tag{7}$$

From equations (6) and (7), α_1 can be found to be

$$\alpha_1 = [(c_s/c_s')^{1/2} - 1]\sin\alpha \tag{8}$$

For a wing, the sectional leading-edge thrust coefficient (ref. 19) can be shown to be

$$c_t = (\pi/2)C^2(1 - M_\infty^2\cos^2\Lambda_{le})^{1/2}/\cos\Lambda_{le} \tag{9}$$

where C is the leading-edge singularity parameter and can be written as

$$C = K'(\sin\alpha + \alpha_1) \tag{10}$$

similar to equation (6). If C_1 is C at α_s, then

$$C_1 = C(\sin\alpha_s + \alpha_1)/(\sin\alpha + \alpha_1) \tag{11}$$

The expression for the leading-edge drag can be found in reference 20. By equating the leading-edge drag to the leading-edge thrust at α_s, it is obtained that

$$\pi \frac{r_o}{c} \frac{\cos\Lambda_{le}}{(1 - M_\infty^2\cos^2\Lambda_{le})^{1/2}} = \frac{\pi}{2} C^2 \frac{(\sin\alpha_s + \alpha_1)^2}{(\sin\alpha + \alpha_1)^2} (1 - M_\infty^2\cos^2\Lambda_{le})^{1/2}/\cos\Lambda_{le}$$

from which α_s can be obtained:

$$\alpha_s = \sin^{-1}[\pm \frac{\sin\alpha + \alpha_1}{C} (2 \frac{r_o}{c})^{1/2}\cos\Lambda_{le}/(1-M_\infty^2\cos^2\Lambda_{le})^{1/2} - \alpha_1] \tag{12}$$

where r_o is the leading-edge radius.

With α_s calculated, the remaining sectional thrust coefficient at $\alpha > \alpha_s$ is then given by equation (9) with C replaced by C_2, where

$$C_2 = C[\sin(\alpha - \alpha_s) + \alpha_1]/(\sin\alpha + \alpha_1) \tag{13}$$

Note that c_t must be converted to the sectional suction coefficient (c_s) before the latter is assumed to become the vortex lift through the method of suction analogy. The relation between c_t and c_s for a cambered wing was derived in reference 5.

The above consideration has been applied to wings in both subsonic and supersonic flows with good success. In the supersonic flow, the wing must have a subsonic leading edge to produce the vortex lift. Some correlation with data was shown earlier in figures 4 and 5.

BODY VORTEX LIFT

If the aspect ratio of a slender thick wing is reduced, eventually it becomes a slender body. If the method of suction analogy is applicable to the former, it should also be applicable to the latter. Based on this understanding, the following method for calculating body vortex lift was developed. The method is based on the following assumptions and procedures.

(a) The attached-flow solution is obtained with the axial distribution of G. N. Ward's vortex multiplets (ref. 21). The boundary condition is satisfied on the body surface.

(b) At any axial station, vortex separation starts at a circumferential location where C_p is minimum and negative. This assumption has been shown to be reasonable (ref. 22). At low angles of attack, C_p may be positive everywhere near the nose. In this case, no vortex separation is assumed to occur. In reference 22, the axial station (x_s) at which the vortex separation starts must be assumed or given by experimental data. Examples of calculated pressure distribution with and without vortex separation are illustrated in figure 8.

(c) At any axial station, the side-force component of the negative C_p in the region assumed to have vortex separation is integrated to produce a sectional side-force coefficient (see fig. 9).

$$c_{sf} = \frac{1}{r(x)} \int_{\theta_{min\ p}} r(x) C_p \sin\theta d\theta \qquad (14)$$

The side force obtained is assumed to be the suction force produced by the separated vortex. This suction force is assumed to be acting at θ_c (fig. 10) where

$$\theta_c = \theta_{min\ p} - \Delta\theta \qquad (15)$$

$$\Delta\theta = h\, c_{sf} \qquad (16)$$

Equations (15)-(16) imply that the vortex action point is located at a distance from $\theta_{min\ p}$ being proportional to the suction force:

$$\Delta s = r\Delta\theta = h\ r\ c_{sf} \tag{17}$$

Based on equation (4), h should be

$$h = 1/4f^2 \tag{18}$$

To determine an appropriate value for f, data in reference 23 as presented in figure 11 are used. Applying the same method as used in figure 2, f is determined to be 0.70. For simplicity, f will be taken to be $1/(2)^{1/2}$ in subsonic flow. In supersonic flow, no data were available for correlation so that an empirical value will be used. In summary, the following values for h will be used in the present method:

$$\begin{aligned} h &= 0.5 \quad , M_\infty < 1.0 \\ &= 3.0 \quad , M_\infty > 1.0 \end{aligned} \tag{19}$$

With θ_c calculated from equation (15), the sectional normal force coefficient due to the vortex suction is given by

$$c_{n,v} = c_{sf}\cos\theta_c \tag{20}$$

(d) Similar to a wing, the augmented body vortex lift exists whenever the planview of a body is not of the delta type. The concept used in calculating the augmented vortex lift for a wing (ref. 4) is also applicable for a body. Thus, if $C_{sf,N}$ is the total suction force coefficient from the nose portion, then the augmented normal force coefficient ($C_{N,vA}$) is given by

$$C_{N,vA} = \tilde{c}\ C_{sf,N}\cos\theta_A/\ell_N \tag{21}$$

where $\tilde{c}$ is the length over which the nose vortex passes and ℓ_N is the nose length. The term θ_A is the location of augmented vortex action point and is assumed to be equal to θ_c at the body shoulder.

Calculated results for an ogive cylinder at $M_\infty = 0.3$ are compared with data in figure 12. The effect of Reynolds number is seen to increase the loading. In references 22 (ref. 24), different axial locations of

initial separation were assumed for different Reynolds numbers. The present results are seen to agree well with the data of higher Reynolds number. This is expected because an inviscid theory, such as the present one, is to simulate the flow field of infinite Reynolds number.

In figure 13 (ref. 25), results for a circular-arc-cylinder body at $M_\infty = 1.6$ are presented. It is seen that the calculated results agree well with data up to $\alpha = 32$ deg. Above $\alpha = 32$ deg at $M_\infty = 1.6$ or $\alpha \geq 15$ deg at $M_\infty = 2.3$ (not shown), the normal force is always underpredicted. This is probably because at high M_∞ and/or high angles of attack, the present linear theory cannot predict accurately the upper surface expansion and strong shock effect on the lower surface.

CONCLUDING REMARKS

The method of suction analogy, originally developed for a plane wing, was shown to be applicable to cambered wings by using the concept of vortex action point. For a wing with rounded leading edges, the method is still applicable if the delay in initial vortex separation is accounted for. The latter can be calculated by Kulfan's method. Kulfan's method was shown to be related to the leading-edge laminar separation. Extension of the suction analogy to predicting the body vortex lift has also been presented.

REFERENCES

1. Polhamus, E. C.: A Concept of the Vortex Lift of Sharp-Edge Delta Wings Based on a Leading-Edge-Suction Analogy. NASA TN D-3767, December 1966.

2. Polhamus, E. C.: Predictions of Vortex-Lift Characteristics by a Leading-Edge Suction Analogy. Journal of Aircraft, Vol. 8, April 1971, pp. 193-199.

3. Lamar, J. E.: Extension of Leading-Edge-Suction Analogy to Wings With Separated Flow Around the Side Edges at Subsonic Speeds. NASA TR R-428, October 1974.

4. Lamar, J. E.: Recent Studies of Subsonic Vortex Lift Including Parameters Affecting Stable Leading-Edge Vortex Flow. Journal of Aircraft, Vol. 24, December 1977, pp. 1205-1211.

5. Lan, C. E., and Chang, J. F.: Calculation of Vortex Lift for Cambered Wings by the Suction Analogy. NASA CR-3449, July 1981.

6. Kulfan, R. M.: Wing Airfoil Shape Effects on the Development of Leading-Edge Vortices. AIAA Paper No. 79-1675, 1979.

7. Kulfan, R. M.: Wing Geometry Effects on Leading Edge Vortices. AIAA Paper No. 79-1872, 1979.

8. Carlson, H. W., and Mack, R. J.: Studies of Leading-Edge Thrust Phenomena. Journal of Aircraft, Vol. 17, December 1980, pp. 890-897.

9. Boyden, R. P.: Effects of Leading-Edge Vortex Flow on the Roll Damping of Slender Wings. Journal of Aircraft, Vol. 8, July 1971, pp. 543-547.

10. Lan, C. E., and Hsu, C. H.: Effects of Vortex Breakdown on Longitudinal and Lateral-Directional Aerodynamics of Slender Wings by the Suction Analogy. AIAA Paper No. 82-1385, 1982.

11. Lan, C. E.: The Unsteady Suction Analogy and Applications. AIAA Journal, Vol. 20, December 1982, pp. 1647-1656.

12. Brennenstuhl, U., and Hummel, D.: Vortex Formation Over Double-Delta Wings. ICAS Paper No. 82-6.6.3, 1982.

13. Squire, L. C.; Jones, J. G.; and Stanbrook, A.: An Experimental Investigation of the Characteristics of Some Plane and Cambered 65° Delta Wings at Mach Numbers from 0.7 to 2.0. British ARC R&M No. 3305, July 1961.

14. Igglesden, M. S.: Wind Tunnel Measurements of the Lift-Dependent Drag of Thin Conically Cambered Slender Delta Wings at Mach Numbers 1.4 and 1.8. Royal Aircraft Establishment of Great Britain, Technical Note No. Aero. 2677, April 1960.

15. Menees, G. P.: Lift, Drag, and Pitching Moment of an Aspect-Ratio-2 Triangular Wing with Leading-Edge Flaps Designed to Simulate Conical Camber. NASA Memo 10-5-58A, December 1958.

16. McCullough, G. B., and Gault, D. E.: Examples of Three Representative Types of Airfoil-Section Stall at Low Speed. NACA TN 2502, September 1951.

17. Stevens, W. A.; Goradia, S. H.; and Braden, J. A.: Mathematical Model for Two-Dimensional Multi-Component Airfoils in Viscous Flow. NASA CR-1843, July 1971.

18. Su, I., and Lan, C. E.: Effect of Round Airfoil Nose on Leading-Edge Suction in Viscous Flow. Technical Report CRINC-FRL-426-3, The University of Kansas Center for Research, Inc., September 1984.

19. Lan, C. E.: A Quasi-Vortex-Lattice Method in Thin Wing Theory. Journal of Aircraft, Vol. 11, September 1974, pp. 518-527.

20. Robinson, A., and Laurmann, J. A.: Wing Theory. Cambridge University Press, 1956.

21. Ward, G. N.: Linearized Theory of Steady High-Speed Flow. Cambridge University Press, 1955.

22. Almosnino, D., and Rom, J.: Calculation of Symmetric Vortex Separation Affecting Subsonic Bodies at High Incidence. AIAA Journal, Vol. 21, March 1983, pp. 398-406.

23. Yanta, W. J.; Wardlaw, A. G., Jr.; and Sternklar, D.: Vortex Asymmetry Development on a Tangent Ogive. NSWC TR-82-394, Naval Surface Weapons Center, Silver Springs, Md., October 1982.

24. Tinling, B. E., and Allen, C. Q.: An Investigation of the Normal Force and Vortex Wake Characteristics of an Ogive-Cylinder Body at Subsonic Speeds. NASA TN D-1297, 1962.

25. Landrum, E. J., and Babb, C. D.: Wind-Tunnel Force and FLow-Visualization Data at Mach Numbers from 1.6 to 4.63 for a Series of Bodies of Revolution at Angles of Attack from -4° to 60°. NASA TM 78813, March 1979.

26. Lighthill, M. J.: Higher Approximations in General Theory of High Speed Aerodynamics. Ed. by W. R. Sears, Princeton University Press, 1954.

27. Liepmann, H. W., and Roshko, A.: Elements of Gasdynamics. John Wiley & Sons, N.Y., 1957.

APPENDIX

CORRECTION FOR NONLINEAR WAVE DRAG

The correction for nonlinear wave drag is based on the difference in predicted results for a two-dimensional flat plate by the linear and exact theories. The linear theory shows that the drag coefficient is given by

$$c_{d_w} = 4\cos\alpha \sin^2\alpha/(M_\infty^2 - 1)^{1/2} \tag{A.1}$$

where the α-terms are not linearized, so that the linearization is with respect to the compressibility effect only. For a three-dimensional wing, α in equation (A.1) is the one associated with the predicted sectional lift coefficient (c_ℓ) as follows:

$$\alpha = \sin^{-1}[c_\ell(M_\infty^2 - 1)^{1/2}]/4 \tag{A.2}$$

The exact theory for a flat plate in supersonic flow shows that the upper surface pressure is given by the Prandtl-Meyer solution (ref. 26, p. 383):

$$C_{p_u} = \frac{2}{\gamma M_\infty^2}\left[\left(\frac{\sin^2\beta}{\gamma - \cos 2\beta}\right)^{\gamma/(\gamma-1)} \Big/ \left(\frac{\sin^2\beta_\infty}{\gamma - \cos 2\beta_\infty}\right)^{\gamma/(\gamma-1)} - 1\right] \tag{A.3}$$

where $\beta_\infty = \sin^{-1}(1/M_\infty)$ and β is found from

$$-\alpha + \beta - \left(\frac{\gamma+1}{\gamma-1}\right)^{1/2}\tan^{-1}\left[\left(\frac{\gamma+1}{\gamma-1}\right)^{1/2}\tan\beta\right] = \beta_\infty - \left(\frac{\gamma+1}{\gamma-1}\right)^{1/2}\tan^{-1}\left[\left(\frac{\gamma+1}{\gamma-1}\right)^{1/2}\tan\beta_\infty\right] \tag{A.4}$$

The lower surface pressure is given by the oblique shock solution (ref. 27, p. 86-88):

$$C_{p_\ell} = 2\sin\beta_s \sin\alpha/\cos(\beta_s - \alpha) \tag{A.5}$$

where β_s is obtained from

$$\tan\alpha = \cot\beta_s \frac{2M_\infty^2\sin^2\beta_s - 2}{(\gamma+1)M_\infty^2 - 2M_\infty^2\sin^2\beta_s + 2} \tag{A.6}$$

From equations (A.3) and (A.5), the pressure differential and the wave drag become

$$\Delta C_p = C_{p_\ell} - C_{p_u} \tag{A.7}$$

$$c_{d_w} = \Delta C_p \sin\alpha \tag{A.8}$$

The difference between the values given by equations (A.8) and (A.1) represents the correction to be added to the predicted sectional drag coefficient by the linear lifting surface theory.

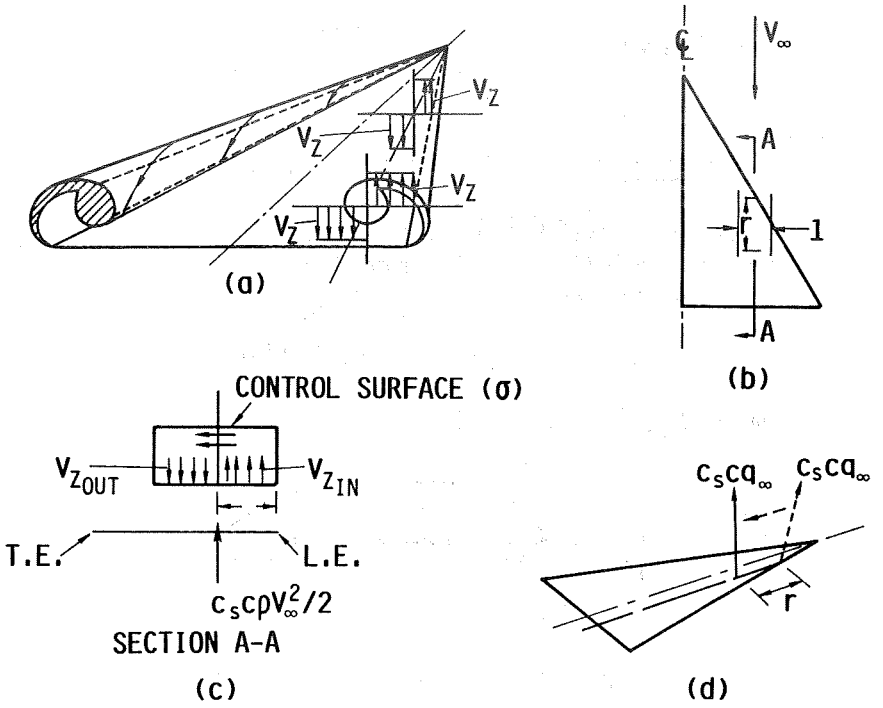

Figure 1. Geometry and flow field for defining vortex action point.

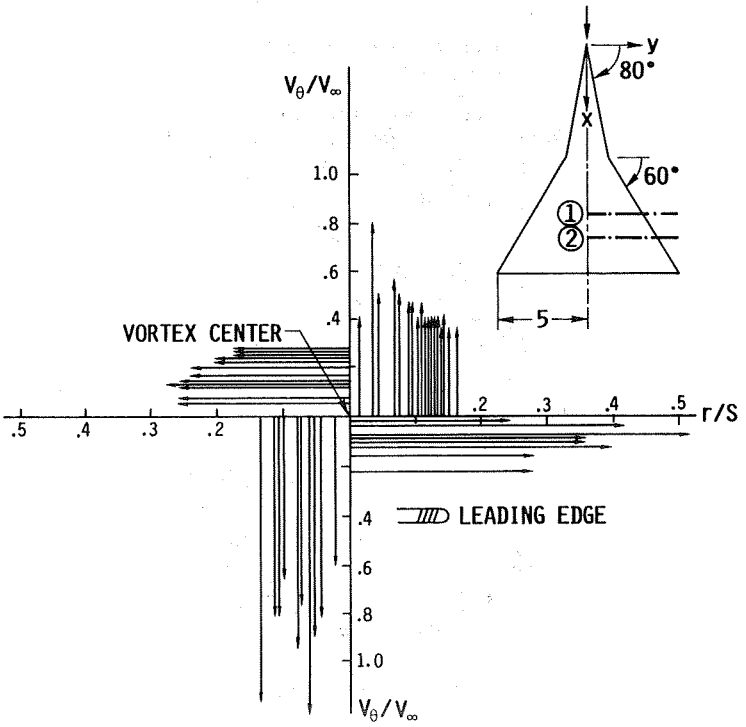

Figure 2. Flow field data at station 1 on a double delta wing at $M_\infty = 0$. Data from ref. 12.

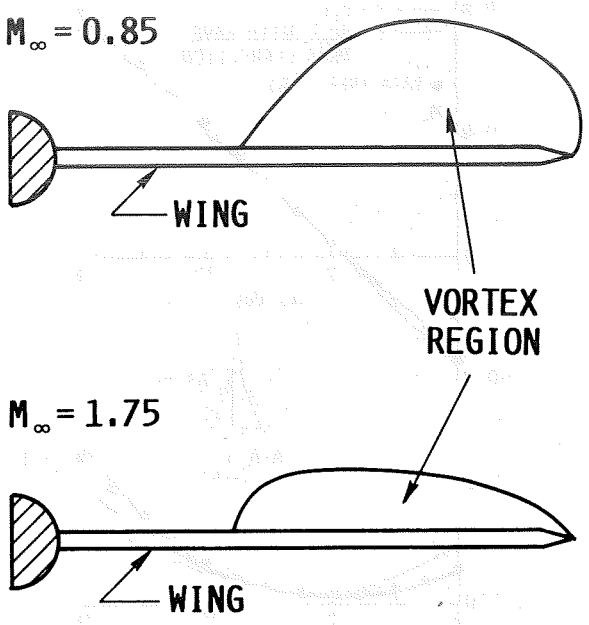

Figure 3. Vortex flow regions on a 65-deg plane wing at subsonic and supersonic speeds. α = 8.1 deg and R_e = 1.5 X 10^6.

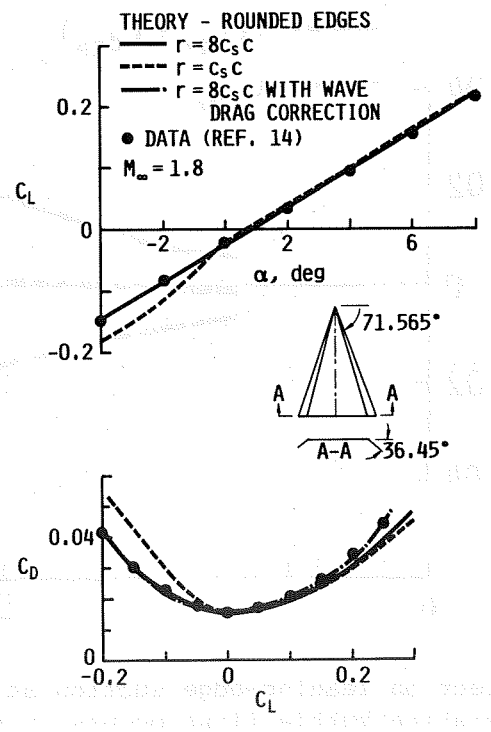

Figure 4. Longitudinal characteristics of a delta wing of aspect ratio 4/3 at M_∞ = 1.8.

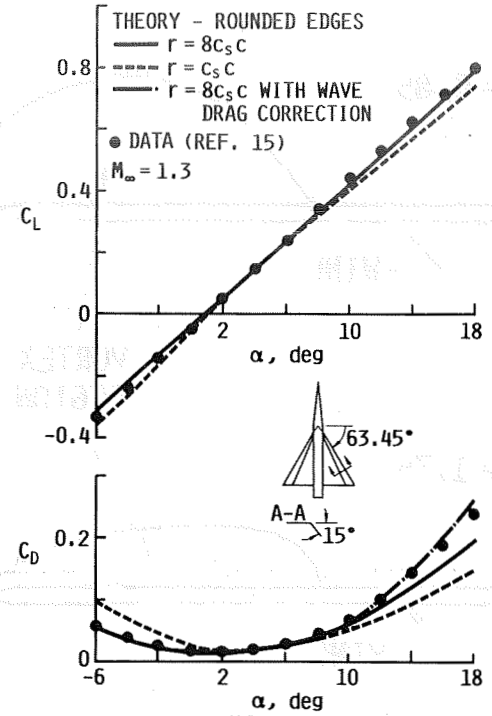

Figure 5. Longitudinal characteristics of a wing-body configuration of aspect ratio 2.0 at M_∞ = 1.3.

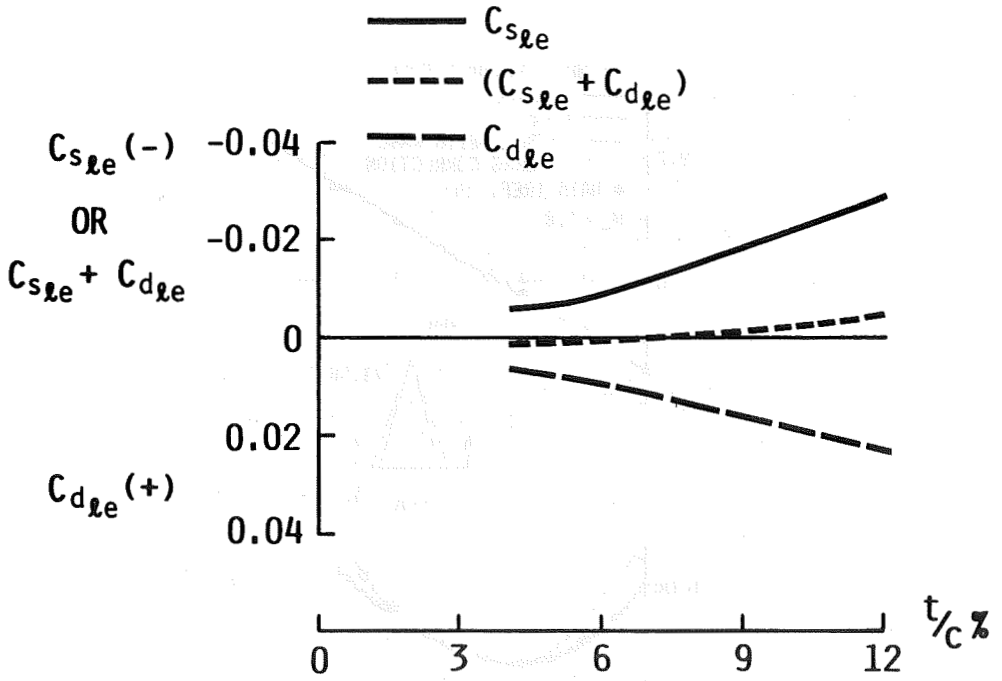

Figure 6. Thickness effect on leading-edge suction at angles of attack at which separation bubble first occurs on symmetrical six-series NASA airfoils. M_∞ = 0.17, R_e = 5.8 X 10^6.

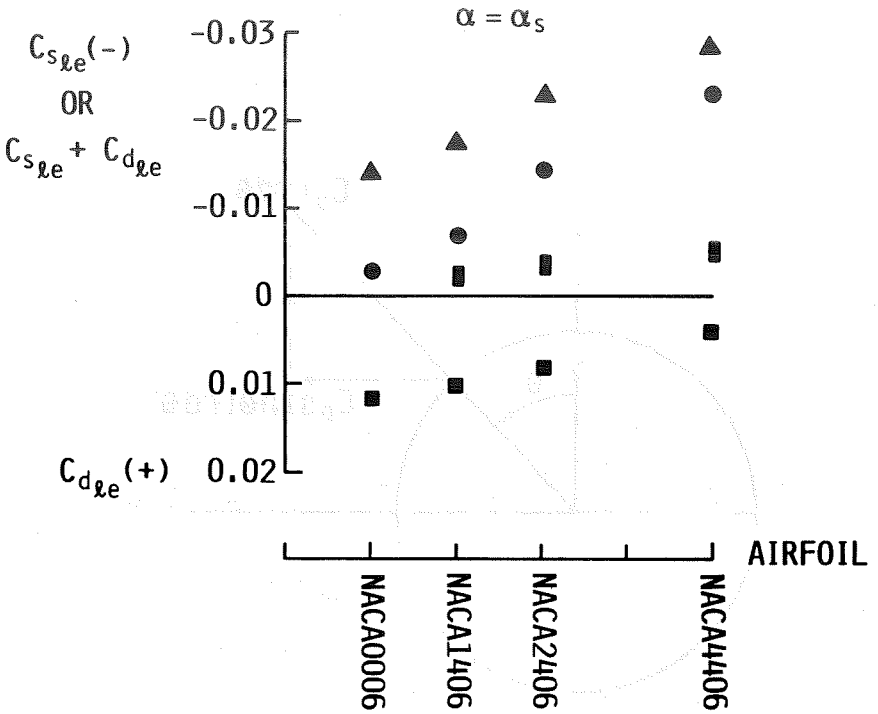

Figure 7. Camber effect on leading-edge suction at angles of attack at which separation bubble first occurs. $M_\infty = 0.17$, $R_e = 5.8 \times 10^6$.

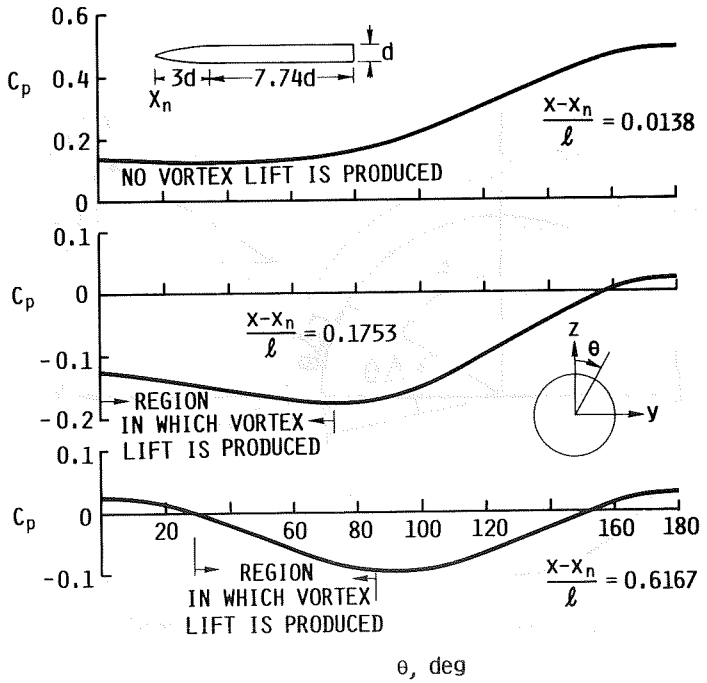

Figure 8. Calculated pressure distribution on an ogive cylinder at $\alpha = 10$ degrees and $M_\infty = 0.3$.

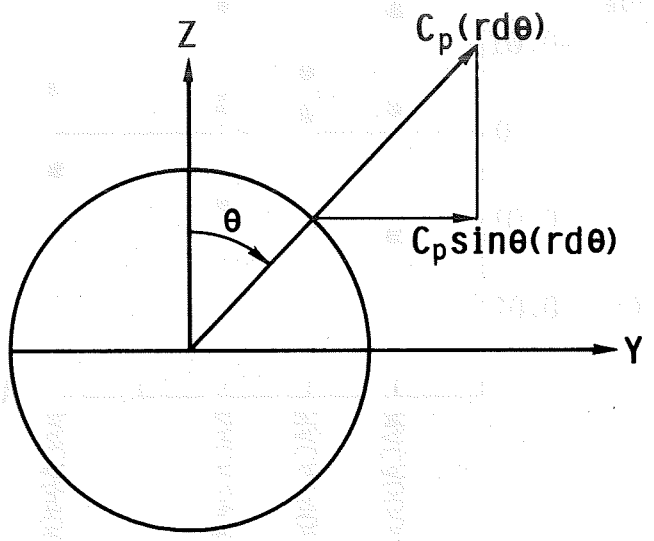

Figure 9. Calculation of positive side force.

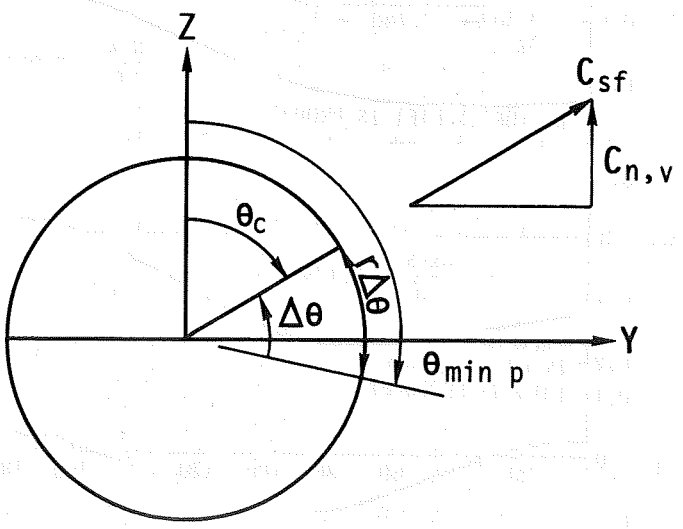

Figure 10. Vortex action point and vortex normal force on a body.

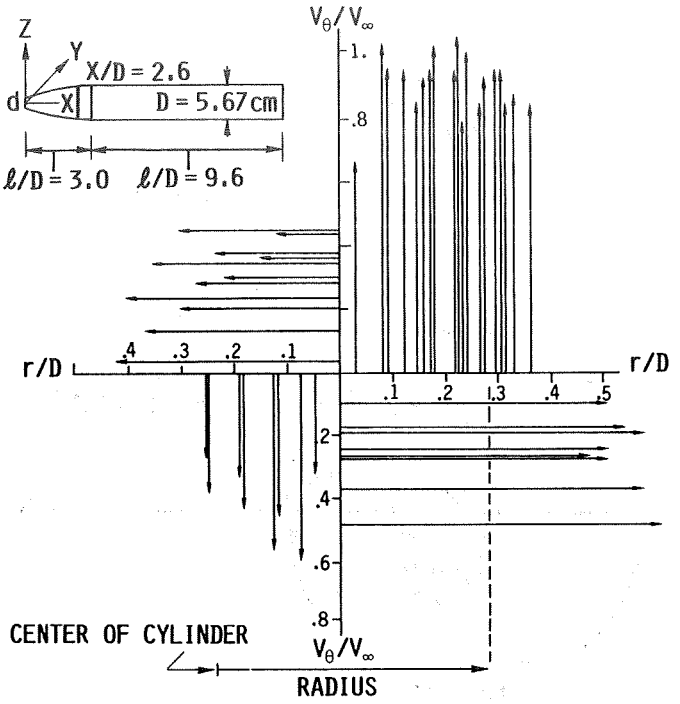

Figure 11. Flow field data from ref. 23 on a tangent ogive body at x/D = 2.6, α = 45 deg and R_e = 1.5 X 10^5.

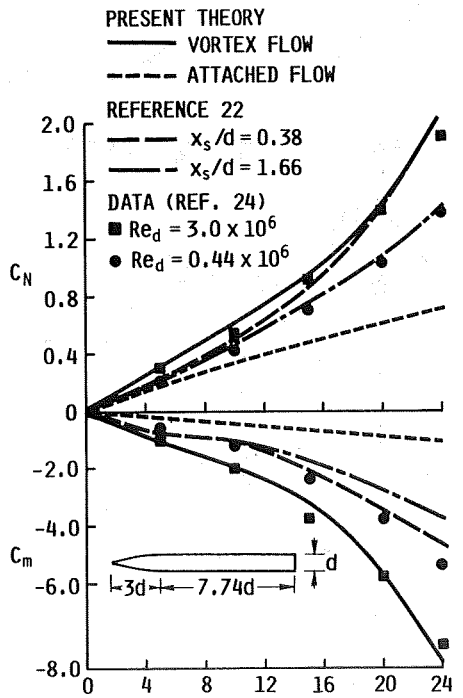

Figure 12. Normal force and pitching moment coefficients for an ogive-cylinder body at M_∞ = 0.3. Moment center at body nose. Reference area = base area and reference length = d.

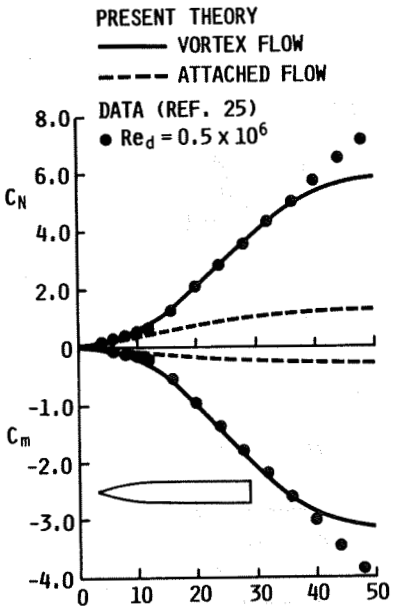

Figure 13. Normal force and pitching moment coefficients for a circular-arc-cylincer body at $M_\infty = 1.6$. Moment center at body nose. Reference area = base area and reference length = body length.